Journal of Sound and Vibration (1997) **208**(3), 367–390

FREE VIBRATION OF SYMMETRICALLY LAMINATED SKEW PLATES

W. Han and S. M. Dickinson

Department of Mechanical and Materials Engineering, The University of Western Ontario, London, Ontario N6A 5B9, Canada

(*Received* 22 *July* 1996, *and in final form* 30 *May* 1997)

A Ritz approach, developed for the analysis of the vibration of thin, laminated, rectangular plates, is extended to apply to symmetrically laminated, composite, skew plates. There is relatively little information available on the vibration of such skew plates, despite their increasing use in the aerospace industry. A convergence study and comparisons with results available from the literature indicate that the approach presented is reliable and accurate. A fairly extensive set of numerical results is given in graphical form, illustrating the influence of different lamination lay-ups, skew angles and edge conditions on the natural frequencies and nodal patterns of a selection of plates.

1. INTRODUCTION

The problem of the free vibration of plates has received a great amount of attention and several hundred papers have appeared on the subject, as may be seen by inspection of the excellent review articles by Leissa [1–7] and Yamada and Irie [8]. A significant number of these papers have dealt with the vibration of thin, skew, isotropic plates, examples of which are those by Barton [9], Nair and Durvasula [10], Bardell [11], Liew and Wang [12] and by McGee and Leissa and their co-workers [13–17]. Laminated, composite, skew plates have received relatively little attention, despite the increasing use of such components in aircraft [18]. Krishnan and Despande [19] studied the free vibration of single layer and cross ply, cantilever, skew plates by using the finite element method. Hosokawa *et al*. [20] used a Green's function approach to treat symmetrically laminated, fully clamped, skew plates. The Ritz method was used by Kapania and Singhvi [21] to study the vibration of tapered thickness, skew, laminated plates and by Kapania and Lovejoy [22] for the analysis of thick cantilevered quadrilateral plates. Singh and Kumar [23] also used the Ritz method to treat four-layer, angle ply, cantilever shallow shells of quadrangular planform, including, as one case, a rhombic shell of zero curvature (a flat plate). Numerical results are given in each of these papers for particular examples but a reasonably comprehensive study of the influences of the boundary conditions, lay-ups and skew angles on the vibration frequencies and mode shapes of plates has not been, substantially, conducted.

In the present work, a Ritz approach, previously described as a hierarchical finite element approach and applied to the free vibration analysis of isotropic rectangular [24] and skew [11] plates by Bardell and to the free [25] and forced vibration [26] of laminated, composite, rectangular plates by Han and Petyt, is extended to apply to the analysis of symmetrically laminated, composite, skew plates. In order to establish the validity of the approach, numerical results were computed for several plates for which results are

0022–460X/97/480367 + 24 $25.00/0/sv971198

available in the literature. These include the cantilevered, isotropic plate, for which very accurate results are available from the work of McGee *et al*. [13], in which special corner functions are included in a Ritz solution to accommodate the stress singularity that occurs at the re-entrant corner of the skew plate. The presence of the stress singularity significantly reduces the rate of convergence of the solution in the absence of the corner functions, as is discussed in detail in references [13–17]. The present approach does not include corner functions but it is demonstrated that, even for highly skewed plates, where the effect is most pronounced, high accuracy is still achieved. Fairly extensive results were then generated for symmetrically laminated, composite, skew plates with various boundary conditions, aspect ratios, skew angles and lamination lay-ups. It is not feasible nor appropriate in an article of this type to present an exhaustive set of results; the number of variables is too high and several of the parameters may be varied infinitely. Consequently, an attempt has been made to provide a representative set of results which serve to illustrate trends of behaviour of the plates with the variation of certain parameters.

2. NUMERICAL APPROACH

The approach used in references [11, 24–26] is here generalized to apply to the vibration analysis of symmetrically laminated, composite, skew plates. Consider a thin, symmetrically laminated, skew plate with side lengths a and b as shown in Figure 1, x-o-y is the skew or oblique co-ordinate system, while the rectangular one is x'-o-y'. ξ-c-η is the non-dimensional, skew co-ordinate system, with c at the centre of the plate. Within the skew system (x-o-y), the plate is bounded by the lines of $x = 0$, $x = a$ and $y = 0$, $y = b$. With the non-dimensional definition of

$$\xi = 2x/a - 1, \qquad \eta = 2y/b - 1, \tag{1}$$

the edges of the plate in the skew co-ordinate system (ξ-c-η) are defined by $\xi = -1$, $\xi = 1$ and $\eta = -1$, $\eta = 1$. For the linear, small amplitude, flexural vibration of symmetrically laminated plates, there is no coupling between the out-of-plane and in-plane displacements, thus only out-of-plane displacement w need be considered. This is taken in the form

$$w = \sum_{r}^{po} \sum_{s}^{po} W_{rs} f_r(\xi) f_s(\eta), \qquad -1 \leqslant \xi, \eta \leqslant 1, \tag{2}$$

where W_{rs} are the generalized displacements, po is the number of the displacement shape functions used in the ξ and η directions, respectively, and f_s and f_r are displacement shape functions which each comprise two sets of polynomials. The first consists of four cubic polynomials which are commonly used in the ordinary finite element method.

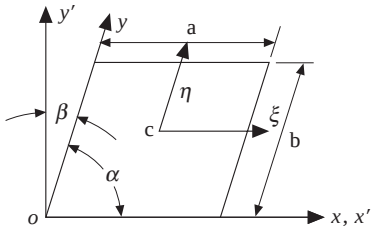

Figure 1. Skew plate and the co-ordinate systems.

They are

$$f_1(\xi) = 1/2 - 3\xi/4 + \xi^3/4, \qquad f_2(\xi) = 1/8 - \xi/8 - \xi^2/8 + \xi^3/8,$$
$$f_3(\xi) = 1/2 + 3\xi/4 - \xi^3/4, \qquad f_4(\xi) = -1/8 - \xi/8 + \xi^2/8 + \xi^3/8. \tag{3}$$

The functions $f_r(\eta)$ ($r = 1, 2, 3$ and 4) are the same with η replacing ξ. The second set is Rodrigues's form of the Legendre polynomials [27] and is generated from

$$f_r(\xi \quad \text{or} \quad \eta) = \sum_{n=0}^{r/2} \frac{(-1)^n(2r - 2n - 7)!!}{2^n n!(r - 2n - 1)!}(\xi \ \text{ or } \ \eta)^{r-2n-1}, \qquad r > 4, \tag{4}$$

where $r!! = r(r-2)\ldots(2 \text{ or } 1)$, $0!! = (-1)!! = 1$, $r/2$ takes its integer part, and ξ and $\eta = -1$ to 1. It can be seen that the order of the polynomials $f_r(\xi \text{ or } \eta)$ generated from equation (4) is $(r-1)$. The first twenty functions are tabulated in the work by Bardell [11].

It should be noted that the polynomials generated by equation (4) have both zero displacement and zero slope at the two ends (ξ and $\eta = -1$ and 1) and hence contribute only internally to the displacement field of the plate. The non-zero boundary displacements of the element are controlled only by the first four displacement shape functions (3). This feature provides significant convenience for the treatment of the various boundary conditions.

The relationship of stress $\{\sigma_x \quad \sigma_y \quad \tau_{xy}\}^T$ and strain $\{\varepsilon_x \quad \varepsilon_y \quad \gamma_{xy}\}^T$ in the skew system for the kth layer of the laminated plate is given by

$$\begin{Bmatrix} \sigma_x \\ \sigma_y \\ \tau_{xy} \end{Bmatrix} = [\mathbf{H}_k] \begin{Bmatrix} \varepsilon_x \\ \varepsilon_y \\ \gamma_{xy} \end{Bmatrix} \tag{5}$$

where

$$[\mathbf{H}_k] = \begin{bmatrix} \sin\alpha & \cos\alpha\cot\alpha & -2\cos\alpha \\ 0 & \operatorname{cosec}\alpha & 0 \\ 0 & -\cot\alpha & 1 \end{bmatrix} [\mathbf{Q}_k] \begin{bmatrix} 1 & 0 & 0 \\ \cot^2\alpha & \operatorname{cosec}^2\alpha & -\cot\alpha\operatorname{cosec}\alpha \\ -2\cot\alpha & 0 & \operatorname{cosec}\alpha \end{bmatrix}, \tag{6}$$

in which the $[\mathbf{H}_k]$ is the reduced stiffness matrix for the kth layer in the skew co-ordinate system and $[\mathbf{Q}_k]$ is the reduced stiffness matrix for the kth layer in the rectangular co-ordinate system [28]. Following the procedure given in reference [25], by simply replacing $[\mathbf{Q}_k]$ with $[\mathbf{H}_k]$, the equation of motion for a thin, symmetrically laminated, skew plate can then be obtained in the form

$$[\mathbf{M}]\{\ddot{\mathbf{q}}\} + [\mathbf{K}]\{\mathbf{q}\} = \{\mathbf{P}\} \tag{37}$$

where $[\mathbf{M}]$ and $[\mathbf{K}]$ are the mass and stiffness matrices, respectively, and $\{\mathbf{q}\}$ and $\{\mathbf{P}\}$ are vectors of generalized displacement, W_{rs}, and applied force, respectively. For free vibration analysis $\{\mathbf{P}\} = 0$. The elements of the mass and stiffness matrices involve integrals of the products of the shape functions and/or their derivatives and are formed by using the computer symbolic manipulation package MAPLE [29]; they are not given here.

After establishment of the stiffness and mass matrices with any given number of displacement shape functions po, the rows and columns in the matrices and vectors corresponding to the constrained degrees of freedoms at the edges of the plate are then deleted. This process is the same as that used in the standard or hierarchical finite element approach.

TABLE 1

Natural frequency parameters Ω for isotropic skew cantilever plates*

or β	*po* ($IxJ + N$)	Mode number DOF	1	2	3	4	5	6
15°	8	48	3·3460	8·1186	20·7512	24·5766	31·6110	48·6098
	12	120	3·3439	8·1149	20·7432	24·5698	31·5952	48·5773
	16	224	3·3434	8·1144	20·7414	24·5685	31·5937	48·5741
	20	360	3·3432	8·1142	20·7406	24·5681	31·5932	48·5734
		(Least [13])	(3·3431)	(8·1145)	(20·7406)	(24·5700)	(31·5952)	(48·5841)
45°	8	48	2·2625	5·6727	13·5628	15·9245	25·4170	29·6205
	($7 \times 7 + 0$)	(49)	(2·2608)	(5·6675)	(13·5448)	(15·8822)	(25·5198)	(29·6619)
	12	120	2·2563	5·6363	13·4990	15·7821	25·3584	29·5500
	16	224	2·2549	5·6281	13·4889	15·7614	25·3560	29·5428
	20	360	2·2542	5·6254	13·4863	15·7563	25·3554	29·5392
	($7 \times 7 + 2$)	(51)	(2·2526)	(5·6239)	(13·4882)	(15·7570)	(25·5040)	(29·6312)
	($7 \times 7 + 10$)	(59)	(2·2526)	(5·6237)	(13·4842)	(15·7524)	(25·3740)	(29·5553)
	($8 \times 8 + 2$)	(66)	(2·2526)	(5·6235)	(13·4841)	(15·7524)†	(25·3696)	(29·5538)
75°	8	48	0·4570	1·7863	3·6676	6·2843	6·8679	10·0637
	12	120	0·4176	1·6943	3·3733	5·2390	6·4540	8·2995
	16	224	0·4090	1·6762	3·3285	5·0341	6·4130	8·2037
	20	360	0·4062	1·6704	3·3080	4·9541	6·4007	8·1714
	($7 \times 7 + 20$)	(69)	(0·4035)	(1·6628)	(3·2659)	(4·8661)	(6·3917)	(8·2483)

† Obtained by using ($7 \times 7 + 10$). Result for ($8 \times 8 + 2$) is 15·7525.

TABLE 2

Convergence study for the 5-layer angle-ply plate, B.C. = C–C–C–C, $\theta = 0^\circ$, $a/b = 1{\cdot}0$

		$\beta = 0^\circ$					$\beta = 60^\circ$				
po	DOF	Ω_1	Ω_2	Ω_3	Ω_4	Ω_5	Ω_1	Ω_2	Ω_3	Ω_4	Ω_5
10	36	23·852	29·715	41·762	60·229	62·974	43·592	67·911	97·483	105·07	132·93
12	64	23·852	29·715	41·721	59·968	62·974	43·576	67·884	97·268	104·91	131·05
14	100	23·852	29·715	41·721	59·963	62·974	43·574	67·878	97·265	104·89	130·98
16	144	23·852	29·715	41·721	59·963	62·974	43·573	67·877	97·265	104·88	130·97
18	196	23·852	29·715	41·721	59·963	62·974	43·573	67·876	97·265	104·88	130·97
20	256	23·852	29·715	41·721	59·963	62·974	43·573	67·876	97·265	104·88	130·97

TABLE 3

Convergence study for the 5-layer angle-ply plate, B.C. = C–C–C–C, $\theta = 30^\circ$, $a/b = 1{\cdot}0$

		$\beta = 0^\circ$					$\beta = 60^\circ$				
po	DOF	Ω_1	Ω_2	Ω_3	Ω_4	Ω_5	Ω_1	Ω_2	Ω_3	Ω_4	Ω_5
10	36	22·713	36·548	54·014	57·207	70·118	52·681	86·175	120·20	125·89	161·76
12	64	22·713	36·546	54·011	57·155	70·078	52·658	86·165	119·94	125·51	159·56
14	100	22·713	36·546	54·011	57·154	70·076	52·653	86·165	119·93	125·46	159·49
16	144	22·713	36·546	54·011	57·154	70·076	52·651	86·165	119·93	125·45	159·49
18	196	22·713	36·546	54·011	57·154	70·076	52·651	86·165	119·93	125·45	159·49
20	256	22·713	36·546	54·011	57·154	70·076	52·651	86·165	119·93	125·45	159·49

TABLE 4

Convergence study for the 16*-layer plate*, *B.C.* = C–C–C–C, $a/b = 1{\cdot}0$

		$\beta = 0^\circ$					$\beta = 60^\circ$				
po	DOF	Ω_1	Ω_2	Ω_3	Ω_4	Ω_5	Ω_1	Ω_2	Ω_3	Ω_4	Ω_5
10	36	22·609	42·280	48·823	70·847	71·660	70·163	104·84	142·10	176·54	189·45
12	64	22·608	42·278	48·820	70·844	71·569	70·048	104·59	139·97	174·69	179·49
14	100	22·608	42·278	48·819	70·844	71·568	70·017	104·58	139·88	174·36	178·88
16	144	22·608	42·278	48·819	70·843	71·568	70·006	104·58	139·88	174·29	178·86
18	196	22·608	42·278	48·819	70·843	71·568	70·002	104·58	139·87	174·27	178·85
20	256	22·608	42·278	48·819	70·843	71·568	70·000	104·58	139·87	174·26	178·85

TABLE 5

Convergence study for the 5*-layer angle-ply plate*, *B.C.* = C–F–F–F, $\theta = 0^\circ$, $a/b = 1{\cdot}0$

		$\beta = 0^\circ$					$\beta = 60^\circ$				
po	DOF	Ω_1	Ω_2	Ω_3	Ω_4	Ω_5	Ω_1	Ω_2	Ω_3	Ω_4	Ω_5
8	48	3·5145	4·7376	9·1110	18·352	22·022	4·2385	7·9845	18·535	27·122	34·449
10	80	3·5144	4·7374	9·1103	18·347	22·021	4·2352	7·9318	18·528	26·983	34·403
12	120	3·5144	4·7374	9·1102	18·347	22·021	4·2342	7·9119	18·525	26·939	34·402
14	168	3·5144	4·7373	9·1101	18·347	22·021	4·2337	7·9032	18·523	26·923	34·402
16	224	3·5144	4·7373	9·1101	18·347	22·021	4·2333	7·8989	18·522	26·916	34·402
18	288	3·5144	4·7373	9·1101	18·347	22·021	4·2330	7·8966	18·521	26·913	34·401
20	360	3·5143	4·7373	9·1101	18·347	22·021	4·2328	7·8953	18·521	26·911	34·401

TABLE 6

Convergence study for the 5*-layer angle-ply plate*, *B.C.* = C–F–F–F, $\theta = 30^\circ$, $a/b = 1{\cdot}0$

		$\beta = 0^\circ$					$\beta = 60^\circ$				
po	DOF	Ω_1	Ω_2	Ω_3	Ω_4	Ω_5	Ω_1	Ω_2	Ω_3	Ω_4	Ω_5
8	48	2·5499	5·9552	12·642	16·432	21·572	3·2603	9·2735	20·365	27·618	40·549
10	80	2·5470	5·9518	12·630	16·425	21·550	3·2494	9·2650	20·231	27·421	40·332
12	120	2·5457	5·9506	12·627	16·421	21·544	3·2456	9·2612	20·181	27·351	40·304
14	168	2·5450	5·9500	12·625	16·419	21·542	3·2438	9·2592	20·159	27·321	40·292
16	224	2·5447	5·9497	12·625	16·417	21·540	3·2428	9·2580	20·148	27·306	40·286
18	288	2·5445	5·9494	12·624	16·416	21·540	3·2422	9·2573	20·142	27·297	40·283
20	360	2·5443	5·9493	12·624	16·416	21·539	3·2417	9·2568	20·139	27·293	40·281

TABLE 7

Convergence study for the 16*-layer plate*, *B.C.* = C–F–F–F, $a/b = 1{\cdot}0$

		$\beta = 0^\circ$					$\beta = 60^\circ$				
po	DOF	Ω_1	Ω_2	Ω_3	Ω_4	Ω_5	Ω_1	Ω_2	Ω_3	Ω_4	Ω_5
8	48	2·1909	6·2605	12·568	16·424	21·462	3·2365	10·502	18·884	31·502	38·218
10	80	2·1879	6·2541	12·549	16·422	21·441	3·2112	10·485	18·656	31·069	37·364
12	120	2·1871	6·2510	12·540	16·421	21·431	3·2018	10·477	18·565	30·894	37·172
14	168	2·1868	6·2495	12·536	16·421	21·425	3·1975	10·472	18·522	30·810	37·088
16	224	2·1867	6·2486	12·533	16·421	21·422	3·1951	10·469	18·499	30·765	37·046
18	288	2·1867	6·2482	12·532	16·421	21·420	3·1936	10·467	18·486	30·739	37·023
20	360	2·1867	6·2479	12·531	16·421	21·419	3·1925	10·465	18·478	30·723	37·009

TABLE 8

A comparison of frequency parameters Ω_i with the results from reference [20]. (PS *present study*)

	i									
	1		2		3		4		5	
β	[20]	PS	[20]	PS	[20]	PS	[20]	PS	[20]	PS
0°	21·44	21·44	32·78	32·77	49·55	49·55	52·40	52·39	65·68	65·67
10°	20·06	20·06	33·20	33·20	47·09	47·09	51·77	51·77	63·28	63·28
20°	19·69	19·69	35·49	35·49	43·81	43·81	56·65	56·65	64·28	64·28
30°	20·61	20·61	40·39	40·39	42·96	42·96	63·81	63·81	70·82	70·82
40°	23·53	23·53	45·38	45·38	49·84	49·84	70·73	70·73	82·15	82·16

TABLE 9

Comparison of fundamental frequency parameters K_1 with the results from reference [19], B.C. = F–C–F–F. (*PS*, *present study*)

β	0°	15°	30°	45°
[19]	1.75939	1.78926	1.92397	2.23240
PS ($po = 12$)	1.76397	1.78896	1.92229	2.31894
PS ($po = 20$)	1.76397	1.78895	1.92224	2.31848

3. NUMERICAL RESULTS

In order to establish confidence in the analysis and results, several convergence studies are presented together with comparisons between results obtained using the present analysis and values available from the literature. Subsequently, new results are presented for plates with two different types of lay-up, for a variety of skew angles, aspect ratios and combinations of boundary conditions. With the exception of two sets of results in the comparison studies, the frequency parameters used throughout are Ω_i, where

$$\Omega_i = (\rho h \omega_i^2 a^4/D_0)^{1/2}, \qquad D_0 = E_1 h^3/12(1 - v_{12} v_{21}), \tag{7}$$

in which ρ is the average density of the plate through the thickness, ω_i is the frequency of ith mode, the minor Poisson's ratio $v_{21} = (E_2/E_1)v_{12}$, and E_1 and E_2 are the Young's moduli of elasticity along and perpendicular to the fibre direction, respectively. The laminated plates treated in this paper are unidirectional fibre reinforced, symmetrically laminated, flat plates with uniform thickness. All layers in a given plate have the same

TABLE 10

Comparison with results of reference [23]. ($a/b = 1{\cdot}0$, $a/h = 100$, PS *present study*)

β	θ	Method	Ω_1	Ω_2	Ω_3	Ω_4	Ω_5
105°	15°	[23]	1·0639	2·0762	5·3513	6·6153	8·4729
		PS	1·0278	2·1072	5·7168	6·5542	8·5668
	30°	[23]	0·9671	2·0744	5·3986	6·2356	8·4168
		PS	0·9428	2·1960	5·7422	6·1459	8·5746
120°	15°	[23]	1·1267	2·2652	5·7041	7·1534	9·9549
		PS	1·1165	2·2787	5·9661	7·2389	10·211
	30°	[23]	1·0675	2·2753	5·6874	6·8328	10·091
		PS	1·0460	2·3661	5·5915	6·9066	10·344

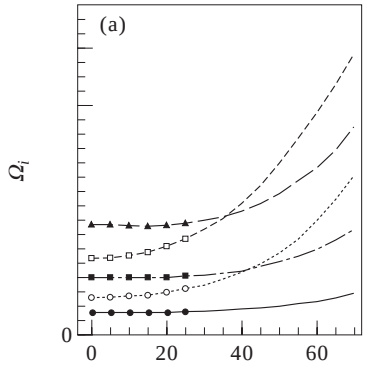
(a)
Ω_i
0
0
20
40
60

the details of which follow, with the first two being for the comparisons with previously published data and the second two being for the new studies.

(1) *Three-layer angle-ply plates*. To compare with results given by Hosokawa *et al*. [20], the three-layer, angle-ply ($[\theta/-\theta/\theta]$, $\theta = 30^\circ$), graphite/epoxy plate used in reference [20] is analysed. The material properties of each layer are: $E_1 = 138$ GPa, $E_2 = 8{\cdot}96$ GPa, $G_{12} = 7{\cdot}1$ GPa, $\nu_{12} = 0{\cdot}30$, where G_{12} is the in-plane shear modulus. In addition, a plate considered by Krishnan and Desphande [19] is considered which has plies ($[\theta/-\theta/\theta]$, $\theta = 90^\circ$) with $E_1/E_2 = 40$, $G_{12}/E_2 = 0{\cdot}6$ and $\nu_{12} = 0{\cdot}25$.

(2) *Four-layer angle-ply plates*. In order to compare with the work of Singh and Kumar [23], the four-layer symmetrically laminated plate ($[\theta/-\theta/-\theta/\theta]$, $\theta = 30^\circ$) used in reference [23] is considered. The material elastic properties are: $E_1/E_2 = 2{\cdot}4474$, $G_{12}/E_2 = 0{\cdot}48458$, $\nu_{12} = 0{\cdot}23$.

(3) *Five-layer angle-ply plates*. The five-layer angle-ply plates considered have lay-up ($[\theta/-\theta/\theta/-\theta/\theta]$, $\theta = 0^\circ$, 15°, 30°, 45°) with the material elastic properties of $E_1/E_2 = 15{\cdot}4$, $G_{12}/E_2 = 0{\cdot}79$, $\nu_{12} = 0{\cdot}30$. (It may be noted that for the case of $\theta = 0^\circ$, the plate is orthotropic). This lamination has been used in the work on rectangular plates by Chow *et al*. [30] and by Han and Petyt [25, 26].

(4) *The* 16*-layer symmetrically laminated graphite/epoxy plate*. The lay-up for this plate is $[45/-45/0/-45/45/45/0/45]_{sym}$. The material properties are $E_1 = 173$ GPa, $E_2 = 7{\cdot}2$ GPa, $G_{12} = 3{\cdot}76$ GPa, $\nu_{12} = 0{\cdot}29$. It should be mentioned that this plate satisfies the condition

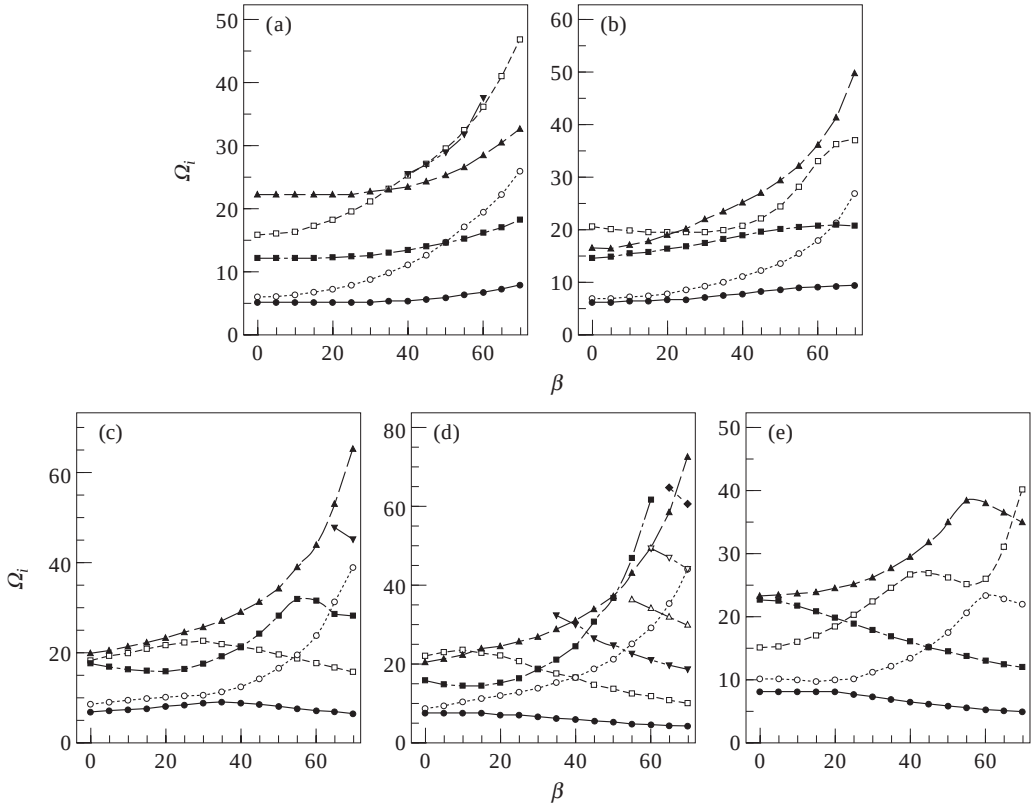

Figure 3. Ω_i versus β curves for the 5-layer angle-ply and 16-layer plates, B.C. = F–F–F–F, $a/b = 1$; (a) $\theta = 0^\circ$, (b) $\theta = 15^\circ$, (c) $\theta = 30^\circ$, (d) $\theta = 45^\circ$, and (e) the 16-layer plate.

of special orthotropy, (that is there is coupling between bending and twisting deformations) and is used as an example in the data sheets of reference [31].

3.1. CONVERGENCE STUDY AND COMPARISON WITH PUBLISHED RESULTS

3.1.1. *Isotropic plates*

In order to investigate the consequence of the omission of corner functions for accommodating the stress singularity which occurs at the re-entrant corner of skewed cantilever plates, an isotropic rhombic plate (aspect ratio $a/b = 1$) is considered. This problem has been treated in detail by McGee *et al*. [13], who presented very accurate results for plates with various skew angles. They showed that the rate of convergence of the Ritz solution for the lower modes of vibration, particularly the fundamental, is significantly reduced for highly skewed plates if the stress singularity is not accounted for by the inclusion of special (corner) functions in the assumed displacement series. The present solution, as with most Ritz solutions, does not include these functions. A convergence study is presented in Table 1 for the first six modes of vibration for the cantilever plate with skew angles 15, 45 and 75 degrees. The frequency parameter employed, $\Omega^* = \Omega_i \cos^2 \beta$, is equivalent to that used in reference [13] and the quantities *po* and DOF are the number of displacement functions used in each direction in the present solution and the corresponding degrees of freedom, respectively. The values in parentheses () are those given by McGee *et al*. [13] as obtained by using $I \times J$ simple polynomials in the displacement function plus N corner functions, resulting in $(I \times J + N)$ degrees of

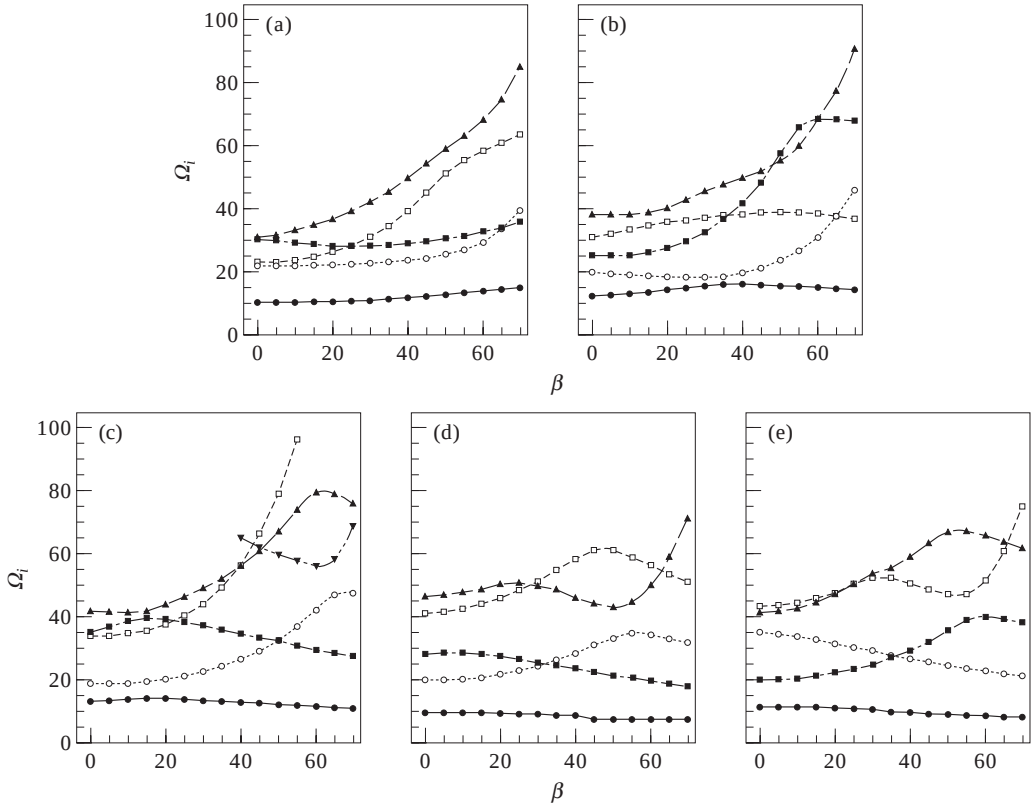

Figure 4. Ω_i versus β curves for the 5-layer angle-ply and 16-layer plates, B.C. = F–F–F–F, $a/b = 2$; (a) $\theta = 0^\circ$, (b) $\theta = 15^\circ$, (c) $\theta = 30^\circ$ (the points after $\beta = 50$ are not shown for mode 3), (d) $\theta = 45^\circ$, and (e) the 16-layer plate.

freedom. The last row in each section gives the lowest and hence most accurate result (by virtue of the upper bound characteristic of the Ritz method) obtained by McGee *et al*. The value of $(I \times J + N)$ used to compute the lowest values for the 15° case was not specified but it was inferred from the text that it was probably $(8 \times 8 + 2)$, giving 66 DOF. Inspection of the table reveals that as either the skew angle or the mode number increases, the rate of convergence of the present solution decreases. For the 15° case, convergence is rapid and the most converged results are very close to those of McGee *et al*. and superior in some cases. This would be expected as the effect of the stress singularity is not significant for small skew angles [13] and many more terms were taken in the present solution than in that by McGee *et al*. For the 45° case, it can be seen that the rate of convergence of the present solution is reasonable but, for the first two modes, a very large number of terms would need to be taken in order to arrive at the results obtained with the corner functions. However, even for the worst case, the fundamental mode, the percentage difference between the $po = 20$ result and the corner function result is only 0·07% which, from a practical viewpoint, is negligible. For modes 5 and 6, the present values are lower and hence more accurate than those of McGee *et al*. For the 75° case (an extremely skewed plate), the rate of convergence remains reasonable and the agreement with the results from reference [13] is excellent. The difference for the fundamental mode is 0·7% and for the worst case (mode 4) it is 1·8%. For mode 6, the present solution is lower by 1%.

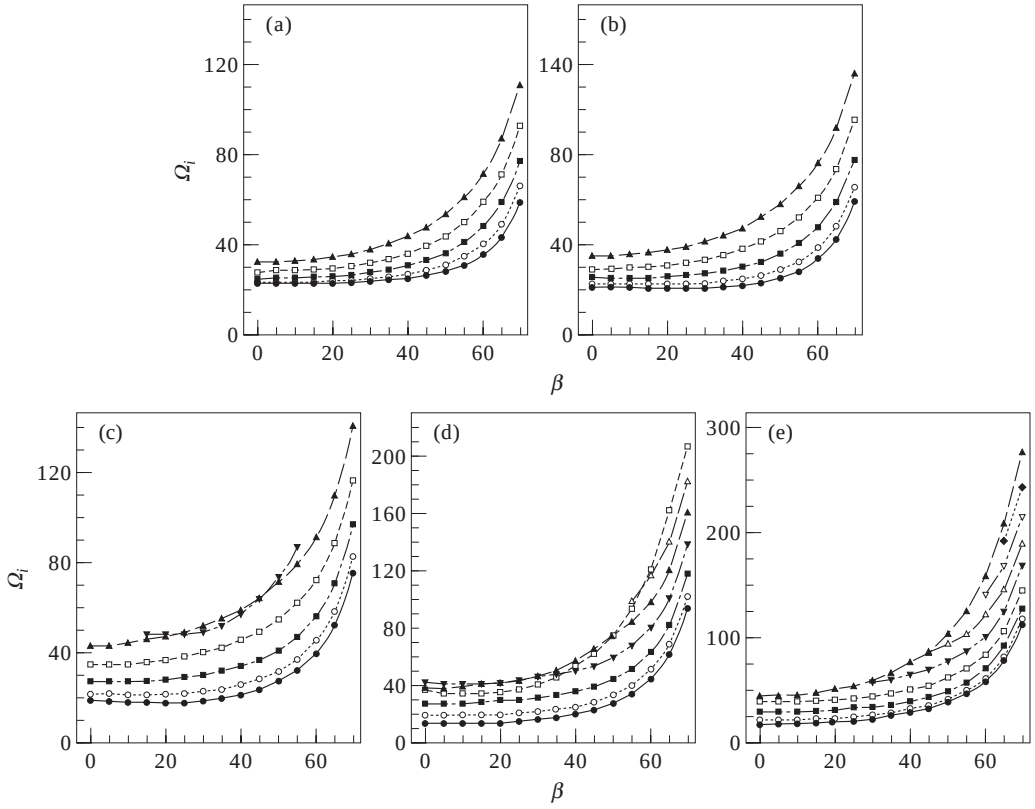

Figure 5. Ω_i versus β curves for the 5-layer angle-ply and 16-layer plates, B.C. = C–C–C–C, $a/b = 0{\cdot}5$; (a) $\theta = 0°$, (b) $\theta = 15°$, (c) $\theta = 30°$, (d) $\theta = 45°$, (six modes plotted) and (e) the 16-layer plate.

It is recognized that the use of corner functions in the present solution would enhance the rate of convergence for some plates. However, for the purposes of this work, the accuracy achieved in their absence was considered more than adequate, making the reasonable assumption that the effect of the stress singularity will not be greatly magnified for laminated plate problems.

It should be mentioned that only the cantilever case has been examined here but the corner stress singularity occurs for other plates, such as simply supported or simply supported/clamped skew plates, where it is the obtuse angle corners that are of concern [16, 17]. It is believed that the present solution will behave in a manner similar to that exhibited here and no further convergence studies were conducted for the isotropic plate.

3.1.2. *Laminated plates*

Three rhombic plates ($a = b$) having the 5- and 16-ply lay-up are considered for two skew angles $\beta = 0^\circ$ (rectangular plate) and $\beta = 60^\circ$ (highly skewed plate). Two fibre orientations are used for the 5-ply plates: $\theta = 0^\circ$ (the orthotropic case) and $\theta = 30^\circ$. The fully clamped (C–C–C–C) and cantilever (C–F–F–F) cases are treated and the first five non-dimensional natural frequencies Ω_i are shown in Tables 2–7, as obtained by using increasing numbers of polynomials *po* in the displacement series. It can be seen from Tables 2–4 that the rate of convergence for the clamped plate is excellent, even for the highly skewed case. Tables 5–7, for the cantilevered plate show that the rate of convergence is very rapid for the rectangular case and reasonable for the highly skewed case, as would

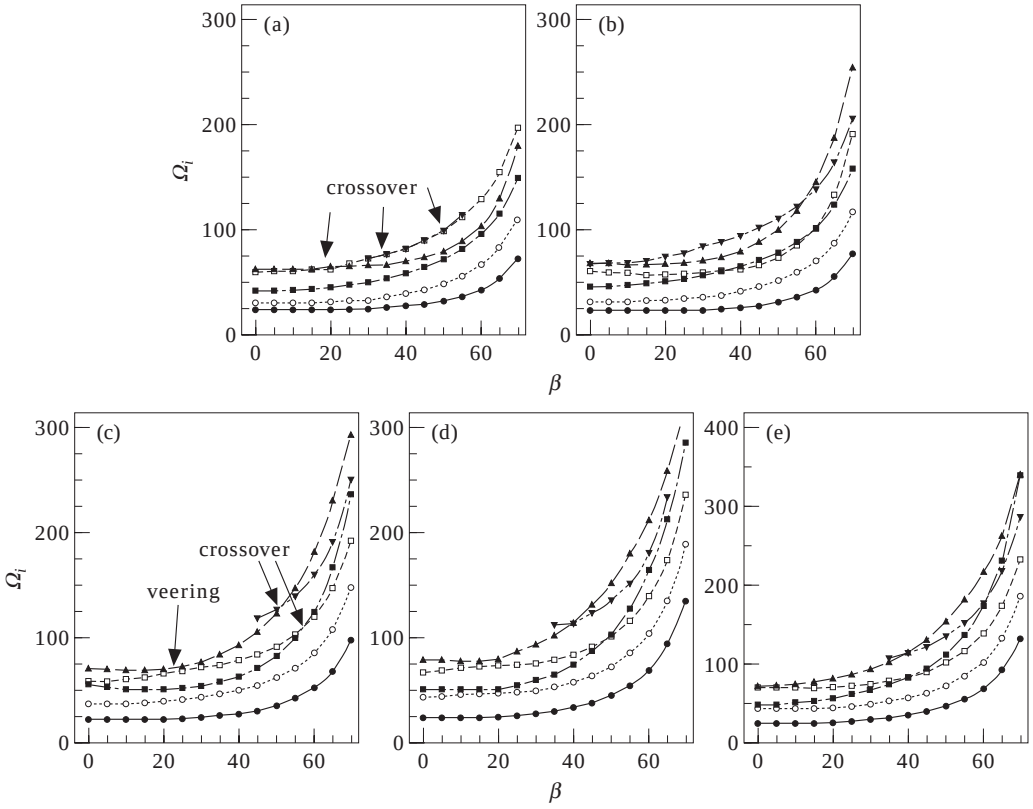

Figure 6. Ω_i versus β curves for the 5-layer angle-ply and 16-layer plates, B.C. = C–C–C–C, $a/b = 1$; (a) $\theta = 0^\circ$, (b) $\theta = 15^\circ$ (special case, with six modes plotted), (c) $\theta = 30^\circ$, (d) $\theta = 45^\circ$, and (e) the 16-layer plate.

be expected from the isotropic plate study. All the frequency predictions, as expected from a Ritz formulation, decrease monotonically with increase in the number of shape functions used. The rate of convergence for the orthotropic 5-ply plates ($\theta = 0^\circ$) is higher than for the $\theta = 30^\circ$, 5-ply plates, which in turn is higher than for the 16-layer plate. In all instances, however, using $po = 20$ appears to be quite adequate for an accurate frequency prediction.

A comparison of the first five frequency parameters with those given in reference [20] is shown in Table 8 for the 3-layer, angle-ply ($[\theta/-\theta/\theta]$, $\theta = 30^\circ$), graphite/epoxy, fully clamped, rhombic plate ($a/b = 1$) with skew angle $\beta = 0$ to 40° (40° is the maximum skew angle used in reference [20]). The present solution results were obtained using both $po = 16$ (144 DOF) and $po = 20$ (256 DOF) and they agreed identically to the number of figures given. They also agree almost identically with those from reference [20], where the method used is very different from that used in this paper.

A second comparison is shown in Table 9, where the fundamental frequency parameters K_1 for 3-layer, cross-ply $[0^\circ/90^\circ/0^\circ]$ cantilever, rhombic plates are given as obtained from the present study, using $po = 12$ and 20 (with the numbers of DOF being 120 and 360, respectively), and as given by Krishnan and Deshpande [19]. The frequency parameter

$$K_1 = \sqrt{\omega_1^2 \rho h a^4 / \sqrt{D_{11} D_{22}}},$$

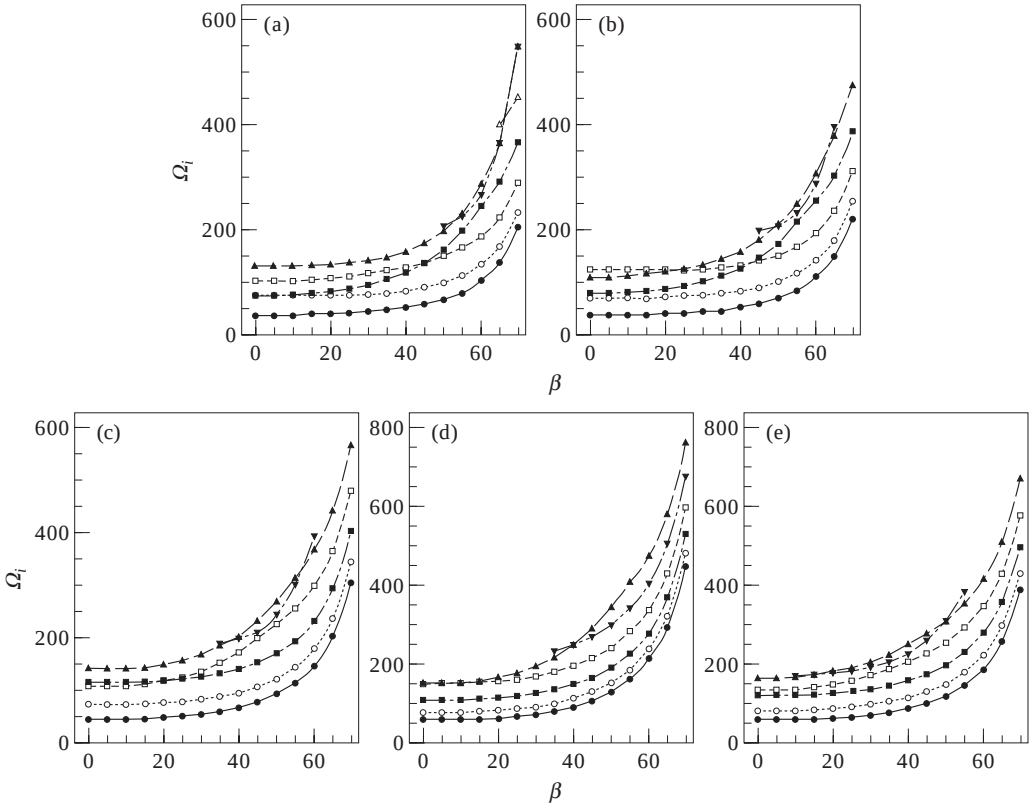

Figure 7. Ω_i versus β curves for the 5-layer angle-ply and 16-layer plates, B.C. = C–C–C–C, $a/b = 2$; (a) $\theta = 0^\circ$, (b) $\theta = 15^\circ$, (c) $\theta = 30^\circ$, (d) $\theta = 45^\circ$, and (e) the 16-layer plate.

where D_{11} and D_{22} are the bending rigidities of the orthropic plate in the direction of the fibres and perpendicular to that direction, respectively. The finite element method with a lumped mass matrix is used in reference [19] and this does not guarantee an upper or lower bound prediction. Transverse shear deflection is also included and hence the solution is applicable to moderately thick plates. For the present comparison, the results for the case $a/h = 100$ are chosen from reference [19] as this corresponds to a thin plate. It can be seen that the agreement between the sets of results from the two sources is very good, giving further confidence in the present analysis.

A third comparison is shown in Table 10, where the first five frequency parameters for the 4-layer, angle-ply, rhombic, cantilever plate, as obtained by Singh and Kumar [23] using a Ritz approach with Bezier polynomials as the displacement functions, are given together with those determined using the present solution. The formulation used in reference [23] is applicable to moderately thick plates and the results quoted from this reference are for the thin plate case, $a/h = 100$. The agreement here is not as close as in the previous two examples. Both methods should yield upper bounds which would suggest that the present method tends to substantially overestimate the frequencies of the second and third modes, particularly for the case $\beta = 105^\circ$. However, on further examination of the results given in reference [23], where a comparison is made with a very accurate Ritz solution by Qatu and Leissa [32] for a square plate with the same lay-up, it appears that the analysis of reference [23] underestimates the frequencies of these two modes (and several others). A comparison of results obtained using the present method and those given

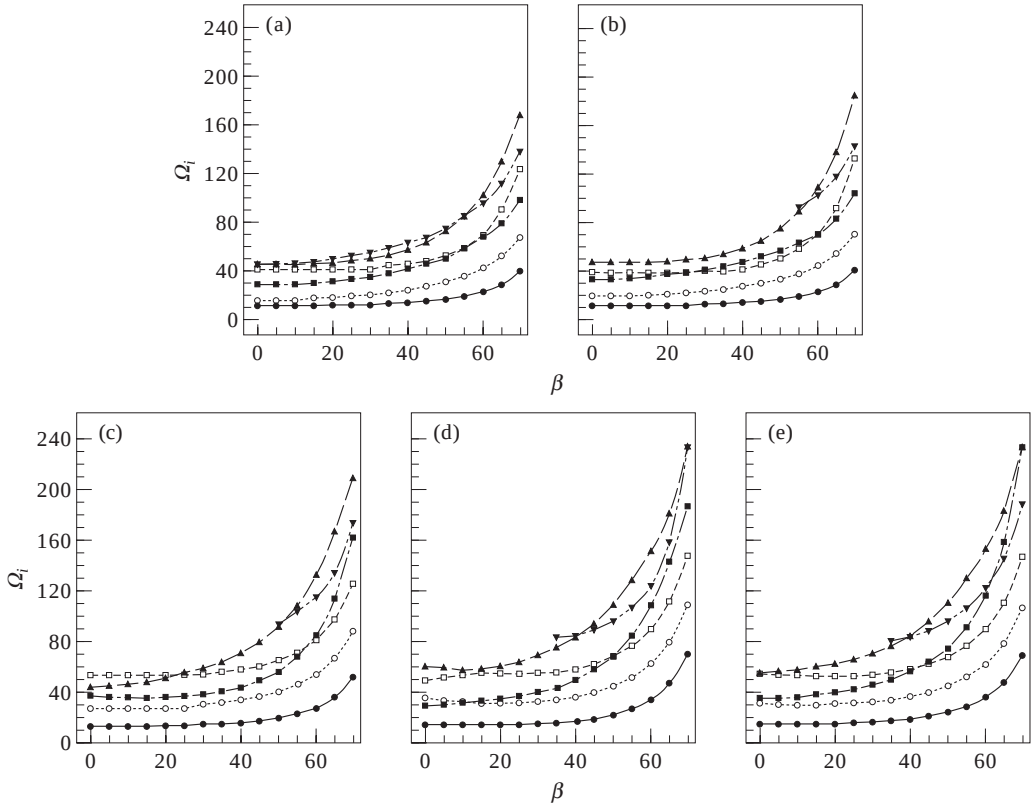

Figure 8. Ω_i versus β curves for the 5-layer angle-ply and 16-layer plates, B.C. = S–S–S–S, $a/b = 1$; (a) $\theta = 0^\circ$, (b) $\theta = 15^\circ$, (c) $\theta = 30^\circ$, (d) $\theta = 45^\circ$, and (e) the 16-layer plate.

by Qatu and Leissa (not presented here) showed close agreement, with the present solution always giving slightly higher values, as anticipated from the upper bound nature of the solution.

Based upon the preceding convergence and comparative studies, the authors believe the present analysis and computational procedure to be reliable and to generate results of reasonable to high accuracy. All further results presented in this paper were generated by using $po = 20$, for which the corresponding degrees of freedom for the F–F–F–F, C–C–C–C, S–S–S–S, C–S–C–S, C–C–S–S and C–F–F–F plates considered are 400, 256, 324, 288, 288, and 360, respectively.

3.2. VARIATION OF THE NON-DIMENSIONAL FREQUENCIES WITH SKEW ANGLES

The relationships between the first few non-dimensional frequencies (Ω_i) and the skew angles (β) of the four different lay-up, 5-layer plates and the one 16-layer plate, with the combinations of boundary conditions mentioned earlier, are now presented graphically. For the F–F–F–F and C–C–C–C cases, the aspect ratios $a/b = 0{\cdot}5$, $1{\cdot}0$ and $2{\cdot}0$ are treated and, for the remainder (S–S–S–S, C–S–C–S, C–C–S–S and C–F–F–F), only $a/b = 1{\cdot}0$ is considered.

In order to produce the Ω_i versus β curves, it was necessary to compute the eigenvalues at certain skew angles (β) and then to plot the curves point by point, joining the points together to give continuous lines. This appears to be trivial but is complicated by the fact that the lines so produced in some cases cross and in others "veer" away. It is

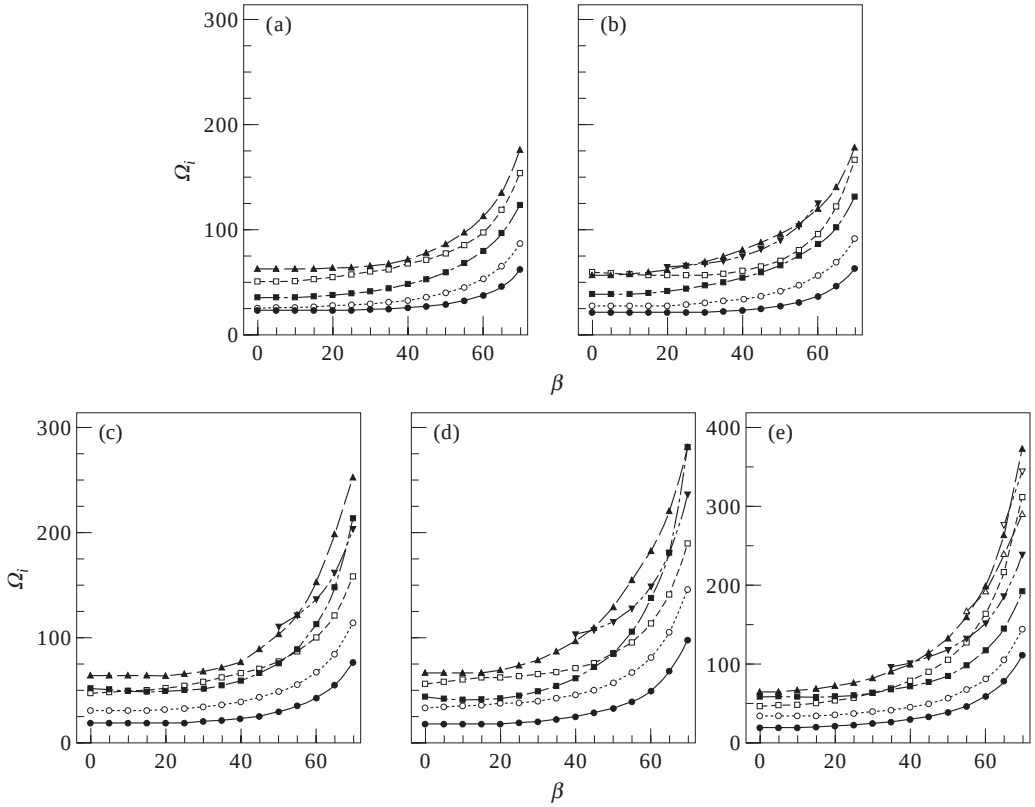

Figure 9. Ω_i versus β curves for the 5-layer angle-ply and 16-layer plates, B.C. = C–S–C–S, $a/b = 1$; (a) $\theta = 0^\circ$, (b) $\theta = 15^\circ$, (c) $\theta = 30^\circ$, (d) $\theta = 45^\circ$, and (e) the 16-layer plate.

difficult in some instances to determine whether veering or crossing actually occurs. Inspection of the smoothness of the curves and the nodal patterns in the vicinity of a crossing or veering was used in order to arrive at the curves presented here. It was observed that, in the vicinity of a crossing, the nodal patterns associated with the two frequencies varied slowly with change of skew angle, whereas where veering occurred, as the two curves approached each other, so the nodal patterns changes significantly with small changes in skew angle, often bearing no resemblance to the "parent" nodal patterns, which were restored as the curves were continued. (This veering/crossing phenomenon is observed in many systems and has been discussed in some detail by Perkins and Mote [33]).

The Ω_i versus β curves presented in all figures in this paper are intended to represent the first five modes of vibration starting from the rectangular plate (that is at $\beta = 0^\circ$). However, with increase in skew angle β, the highest of these five modes may no longer be represented by the fifth curve at that particular skew angle. In this case, the curves corresponding to the modes other than these five are also plotted partially. By presenting the results in this way, the figures not only show the change of the first five modes (as defined at $\beta = 0^\circ$) with increase in skew angle, but also give a picture of higher mode curves crossing. It should be mentioned that, for the purpose of discussion, the curves in the figures are assumed to be numbered in ascending order as they appear at $\beta = 0^\circ$. For example, the third curve in a particular figure is identified as the one that starts as the third curve at $\beta = 0^\circ$ and it may not represent the third lowest frequency at a higher skew angle. The different symbols and classes of lines used in the figures are employed simply to aid

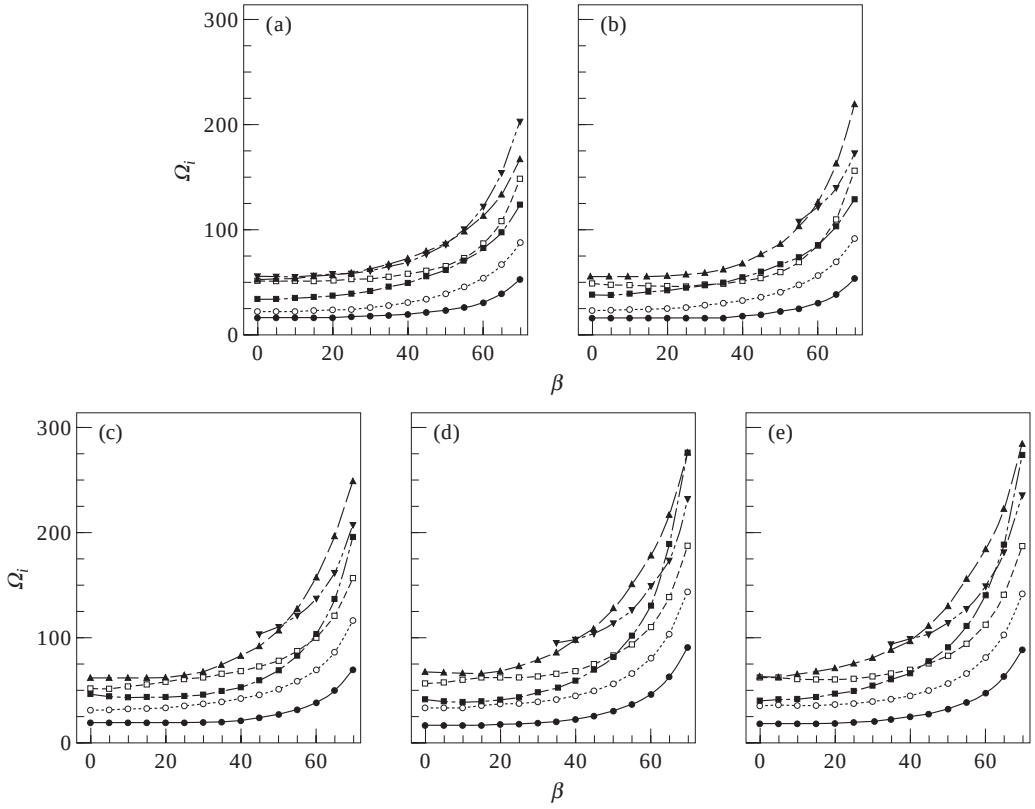

Figure 10. Ω_i versus β curves for the 5-layer angle-ply and 16-layer plates, B.C. = C–C–S–S, $a/b = 1$; (a) $\theta = 0^\circ$, (b) $\theta = 15^\circ$, (c) $\theta = 30^\circ$, (d) $\theta = 45^\circ$, and (e) the 16-layer plate.

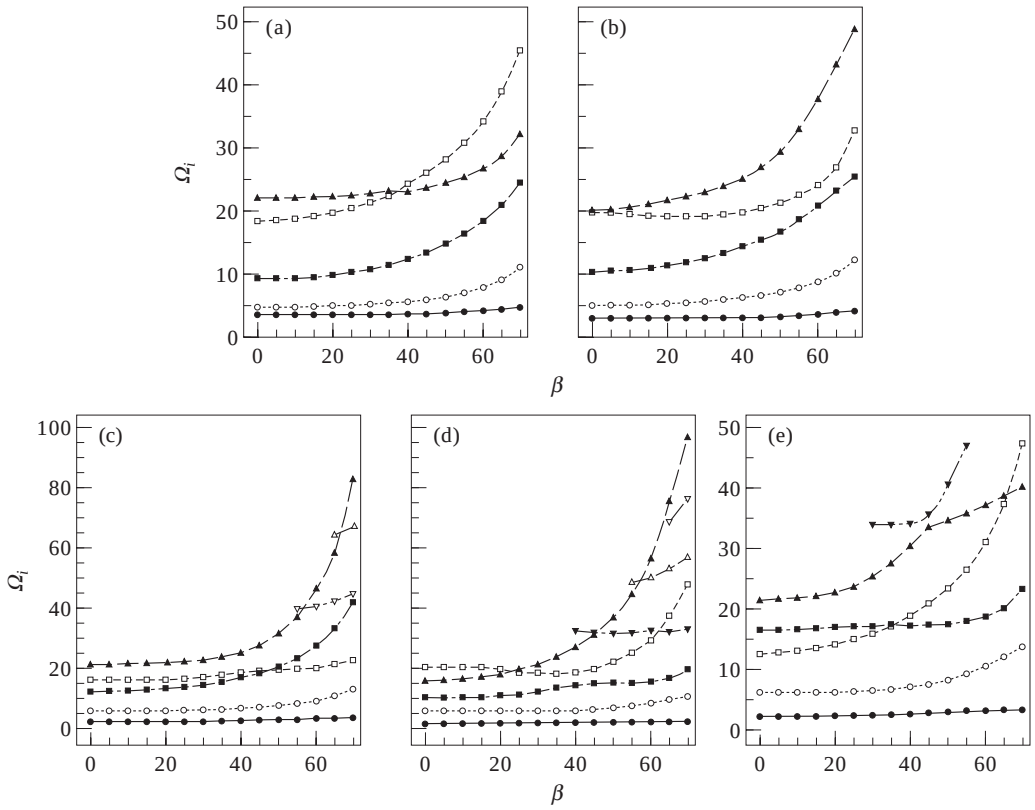

Figure 11. Ω_i versus β curves for the 5-layer angle-ply and 16-layer plates, B.C. = C–F–F–F, $a/b = 1$; (a) $\theta = 0^\circ$, (b) $\theta = 15^\circ$, (c) $\theta = 30^\circ$, (d) $\theta = 45^\circ$, and (e) the 16-layer plate.

the reader to track the frequencies for the various modes and do not identify a particular mode sequence.

Figures 2–4 show the curves for the fully free plates. It may be observed that, for the 5-layer plates with $\theta = 0^\circ$, almost all of the frequency parameters illustrated tend to increase with skew angle β over the range 0°–70°, the most notable exception being the

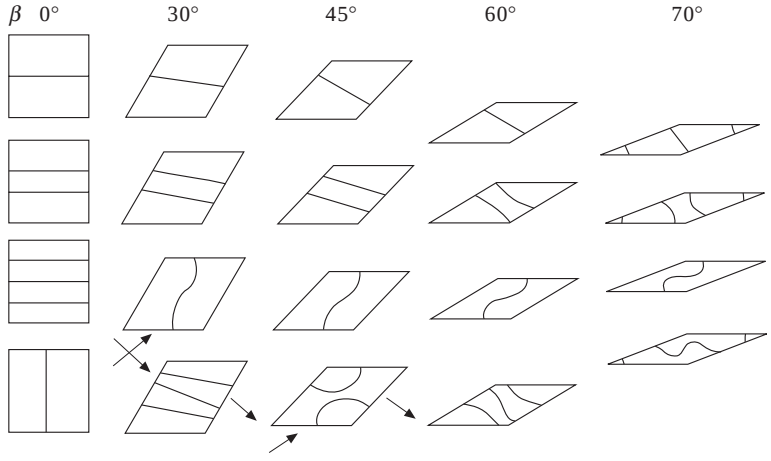

Figure 12. Nodal patterns for the 5-layer angle-ply plate ($\theta = 0^\circ$), $a/b = 1{\cdot}0$, B.C. = C–C–C–C.

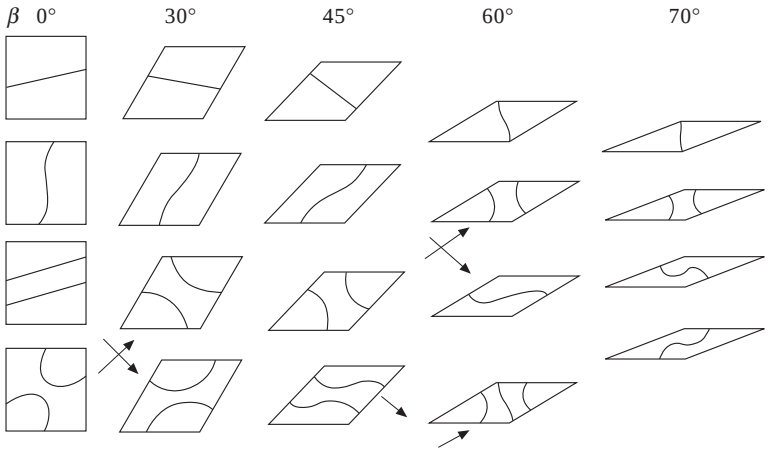

Figure 13. Nodal patterns for the 5-layer angle-ply plate ($\theta = 30^\circ$), $a/b = 1{\cdot}0$, B.C. = C–C–C–C.

fourth curve for $a/b = 2$ (Figure 4(a)). As the fibre orientation angle increases (Figures 2 to 4, (b, c and d)), the behaviour of the curves becomes more complex. Some curves exhibit peaks at particular fibre angles and there is an increasing tendency for crossings of the curves to occur. No clear trend is indicated for the variation of frequency parameter with fibre angle for a given aspect ratio a/b, this being somewhat dependent upon the particular value of skew angle β at which the comparison is being made. As a/b increases, for other quantities being constant, the frequency parameter increases, as would be anticipated since Ω is based upon side length a, which remains constant while b is decreased, resulting in a plate of smaller area which is correspondingly stiffer. The curves for the 16-layer plates are shown in Figures 2–4(e) and these somewhat resemble those obtained for the $\theta = 30^\circ$ or 45° plates.

Figures 5–7 show the curves for the fully clamped plates (C–C–C–C). Each set of curves has similar characteristics. In almost all cases, the frequency parameters increase relatively slowly with increase in skew angle over approximately the first 45°, after which a relatively rapid increase is observed. A few of the curves exhibit slight decreases in frequency parameter over the lower skew angles, after which they too increase rapidly with β. The rapid increase in frequency parameter with increase of skew angle above approximately

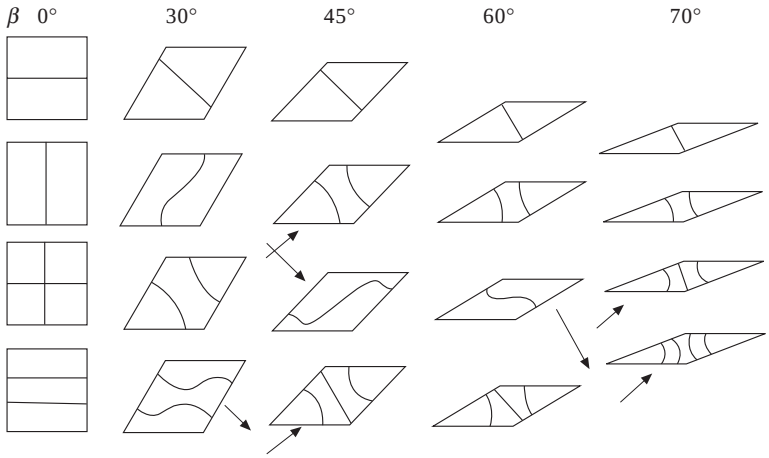

Figure 14. Nodal patterns for the 16-layer angle-ply plate, $a/b = 1{\cdot}0$, B.C. = C–C–C–C.

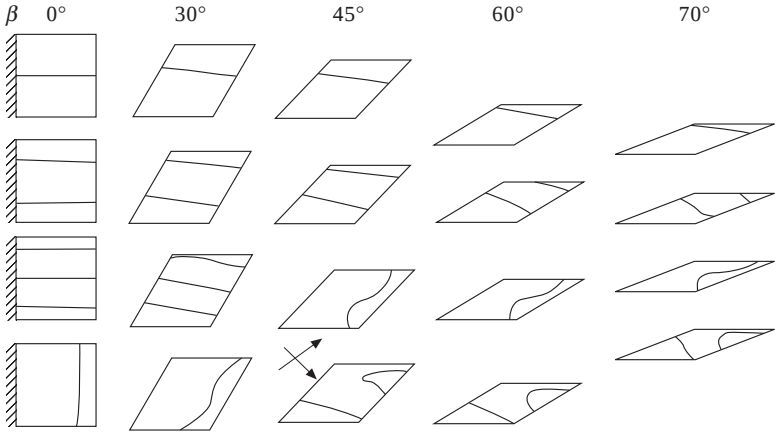

Figure 15. Nodal patterns for the 5-layer angle-ply plate ($\theta = 0^\circ$), $a/b = 1{\cdot}0$, B.C. = C–F–F–F.

45° is largely attributable to the fact that the plate size decreases with increase in skew angle; the edges approach each other and considerably stiffen the plate through the clamping effect. There is no clear trend in the variation of the frequency parameter with the change in fibre orientation θ; the frequencies for some modes for a particular plate decrease with increase in θ (for example mode 1, $a/b = 0{\cdot}5$, Figure 5) and others increase (for example, mode 5, Figure 5). The frequency parameters for the plates with increasing a/b all tend to increase, which is again mainly attributable to the stiffening effect of decreasing length b while maintaining width a constant.

In Figures 8–10, the respective curves are shown for rhombic plates ($a/b = 1$) with all edges simply supported (S–S–S–S), two parallel edges clamped and the other two simply supported (C–S–C–S), and two adjacent edges clamped and the other two simply supported (C–C–S–S). Apart from the actual magnitude of the frequency parameters, these all exhibit similar characteristics to the equivalent curves for the rhombic clamped plate (Figure 6). Clearly, the more clamped edges that exist, the higher the frequencies of the plate. For the (C–S–C–S) and (C–C–S–S) plates, the sets of curves are very similar but not identical. Although it is not easy to see without overlaying equivalent curves for each plate, it is found that the fundamental frequency for the (C–S–C–S) plate is slightly lower

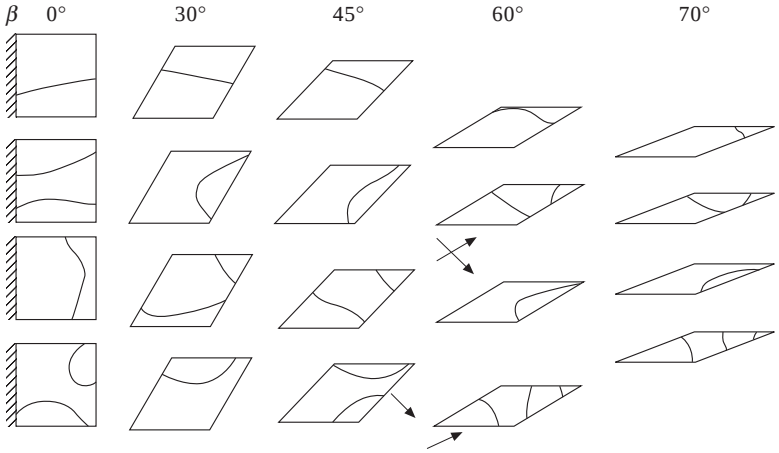

Figure 16. Nodal patterns for the 5-layer angle-ply plate ($\theta = 30^\circ$), $a/b = 1{\cdot}0$, B.C. = C–F–F–F.

than for the equivalent (C–C–S–S) plate for all skew angles and all fibre orientations. Certain other curves are almost identical for the plates with two different boundary conditions (such as those for mode 2), while some are less similar in their behaviour.

The last set of curves shown in this section (Figure 11) is that for the rhombic cantilevered plate (C–F–F–F). Here, for the 5-layer plates, is may be seen that there is a general tendency for the frequency parameter to increase with skew angle, although the fundamental frequency appears to be relatively insensitive. As the fibre angle is increased, so there is an increased tendency for mode crossings to occur, as exhibited by the fully free plate and, to a lesser extent, by the supported plates. The behaviour of the 16-layer plate tends to resemble that of the 5-layer 30° fibre angle, plate.

3.3. NODAL PATTERNS

Nodal patterns are shown in Figures 12–14 for rhombic fully clamped plates and in Figures 15–17 for cantilevered plates, these being support conditions likely to be encountered in practice. The results are for two 5-layer plates ($\theta = 0^\circ$ and 30°) and the 16-layer plate. The fundamental mode in each case exhibits no nodal lines and is thus omitted; the patterns plotted correspond to modes 2–5 in increasing value of frequency. Since, in most cases, the change of the mode shape is relatively small when the skew angle varies from 0° to 30°, no nodal pattern is presented in the range of $0^\circ < \beta < 30^\circ$, although some were generated to help in the construction of the Ω_i versus β curves. The skew angles at which the nodal lines are plotted are $\beta = 0^\circ$, 30°, 45°, 60° and 70°. Where a "crossing" or "veering" has occurred in the frequency parameter/skew angle curves, this is indicated in the nodal pattern figures by arrows.

The nodal patterns shown in Figures 12 correspond to the frequency parameter/skew angle curves shown in Figure 6(a). Inspection of these two figures shows none of the first three modes exhibits crossing or veering tendencies. For the fourth and fifth mode, it may be seen from Figure 12 that a crossing takes place between $\beta = 0^\circ$ and 30°, this may be confirmed by inspection of Figure 6(a). Between $\beta = 30^\circ$ and 60°, a sixth mode (barely perceptible on the scale of Figure 6(a)) comes into play, causing two crossings, one between $\beta = 30^\circ$ and 45° and the other between $\beta = 45^\circ$ and 60°. Examination of Figures 6(c) and 13 further illustrates the crossing and veering phenomena, where it can be clearly seen that crossing takes place between the third and fourth modes and between the fifth and sixth modes in the range $\beta = 45^\circ$ to 60° and that veering takes

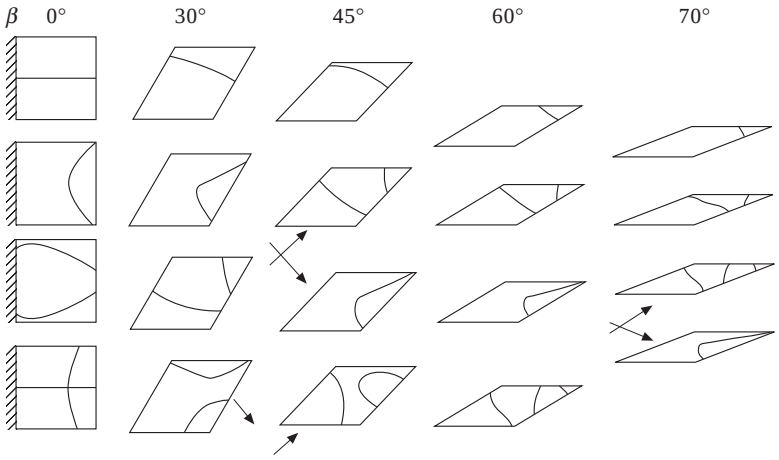

Figure 17. Nodal patterns for the 16-layer plate $a/b = 1{\cdot}0$, B.C. = C–F–F–F.

place between the fourth and fifth modes in the range $\beta = 0^\circ$ to 30°. Inspection of the pairs of Figures 14 and 6(e), 15 and 8(a), 16 and 8(c), and 17 and 8(e) permits similar correlations to be made between the changes in order of nodal patterns and the crossing and veering exhibited in the frequency parameter/skew angle curves. (In order to confirm the validity of the nodal patterns, the mode shapes for a clamped and a cantilever, 5-layer plate, with fibre angle $\theta = 30^\circ$ and skew angle $\beta = 70^\circ$, were generated using the commercial finite element package ABAQUS [34] with an 8×8 mesh of 8-noded shell elements and compared with the patterns shown in Figures 13 and 16. Close agreement was achieved for all nodal patterns given except for the fifth mode of the clamped case at $\beta = 70^\circ$, where three nodal lines similar to the $\beta = 60^\circ$ case were obtained using ABAQUS. The agreement between the natural frequency parameters was also close.)

In general, the nodal patterns of the laminated skew plates shown in Figures 12–17 are somewhat more complicated than those of isotropic skew plates with the same boundary conditions which are illustrated in references [10] and [11].

4. CONCLUDING REMARKS

A Ritz approach has been presented for the study of the free vibration of laminated, composite, skew plates with various boundary conditions, laminations, and side ratios. The convergence rate for the solution has been shown to be reasonably fast and, from comparison with earlier published work, the accuracy and validity of the approach verified. Reasonably extensive numerical results have been presented and the authors believe this to be the most comprehensive investigation on the subject to date. The method presented can be used for the prediction of the free vibration characteristics of arbitrarily symmetrically laminated, skew plates with any combinations of clamped, simply supported and free boundary conditions or corner point supports (not treated here). Recognizing that the approach described is also a single hierarchical finite element solution, if more than one element were to be used, plates involving stepped thickness, line supports, interior point supports and/or cut-outs and plates of different geometries may be studied. The method may be extended to apply to the geometrically non-linear vibration analysis problem, as has been demonstrated for the rectangular plate case by Han and Petyt [35, 36].

ACKNOWLEDGMENTS

The authors wish to thank the Natural Sciences and Engineering Research Council of Canada for the financial support that permitted the conduct of this work and the reviewers for their constructive comments.

REFERENCES

1. A. W. Leissa 1969 *Vibration of plates* (NASA SP-160). Washington, D.C.: U.S. Government Printing Office.
2. A. W. Leissa 1977 *The Shock and Vibration Digest* **9**(10), 13–24. Recent research in plate vibrations, 1973–1976: classical theory.
3. A. W. Leissa 1977 *The Shock and Vibration Digest* **9**(11), 21–35. Recent research in plate vibrations, 1973–1976: complicating effects.
4. A. W. Leissa 1981 *The Shock and Vibration Digest* **13**(9), 11–22. Plate vibration research, 1976–1980: classical theory.
5. A. W. Leissa 1981 *The Shock and Vibration Digest* **13**(10), 19–36. Plate vibration research, 1976–1980: complicating effects.

6. A. W. Leissa 1987 *The Shock and Vibration Digest* **19**(2), 11–18. Plate vibration research, 1981–1985, part I. Classical theory.
7. A. W. Leissa 1987 *The Shock and Vibration Digest* **19**(3), 10–24. Recent studies in plate vibration, 1981–1985, part II. Complicating effects.
8. G. Yamada and T. Irie 1987 *Applied Mechanics Reviews* **40**, 879–892. Plate vibration research in Japan.
9. M. V. Barton 1951 *Journal of Applied Mechanics* **18**, 129–134. Vibration of rectangular and skew cantilever plates.
10. P. S. Nair and S. Durvasula 1973 *Journal of Sound and Vibration* **26**, 1–19. Vibration of skew plates.
11. N. S. Bardell 1992 *Computers and Structures* **45**, 841–874. The free vibration of skew plates using the hierarchical finite element method.
12. K. M. Liew and C. M. Wang 1993 *Computers and Structures* **49**, 941–951. Vibration studies on skew plates: treatment of internal line supports.
13. O. G. McGee, A. W. Leissa and C. S. Huang 1992 *International Journal of Numerical Methods in Engineering* **15**, 409–424. Vibrations of cantilevered skewed plates with corner stress singularities.
14. O. G. McGee, A. W. Leissa and C. S. Huang 1992 *International Journal of Mechanical Sciences* **34**, 63–84. Vibrations of cantilevered skewed trapezoidal and triangular plates with corner stress singularities.
15. O. G. McGee, C. S. Huang and A. W. Leissa 1994 *Computers and Structures* **53**, 667–677. Influence of corner stress singularities and nonstructural mass on the vibrations of cantilevered skewed trapezoidal plates.
16. C. S. Huang, O. G. McGee, A. W. Leissa and J. W. Kim 1995 *Journal of Vibration and Acoustics* **117**, 245–251. Accurate vibration analysis of simply supported rhombic plates by considering stress singularities.
17. O. G. McGee, J. W. Kim, Y. S. Kim and A. W. Leissa 1996 *Journal of Sound and Vibration* **193**, 555–580. Corner stress singularity effects on the vibration of rhombic plates with combinations of clamped and simply supported edges.
18. D. H. Middleton (editor) 1990 *Composite Materials in Aircraft Structures*. New York: Longman Scientific & Technical.
19. A. Krishnan and J. V. Deshpande 1992 *Journal of Sound and Vibration* **152**, 351–358. Vibration of skew laminates.
20. K. Hosokawa, Y. Terada and T. Sakata 1996 *Journal of Sound and Vibration* **189**, 525–533. Free vibrations of clamped symmetrically laminated skew plates.
21. R. K. Kapania and S. Singhvi 1992 *Composites Engineering* **2**, 197–212. Free vibration analysis of generally laminated tapered skew plates.
22. R. K. Kapania and A. E. Lovejoy 1996 *American Institute of Aeronautics and Astronautics Journal* **34**, 1474–1486. Free vibration of thick generally laminated cantilever quadrilateral plates.
23. A. V. Singh and V. Kumar 1996 *Journal of Aerospace Engineering* **9**, 52–57. Vibration of laminated shallow shells on quadrangular boundary.
24. N. S. Bardell 1991 *Journal of Sound and Vibration* **151**, 263–289. Free vibration analysis of a flat plate using the hierarchical finite element method.
25. W. Han and M. Petyt 1996 *Computers and Structures* **61**, 705–712. Linear vibration analysis of laminated rectangular plates using the hierarchical finite element method, Part 1: free vibration analysis.
26. W. Han and M. Petyt 1996 *Computers and Structures* **61**, 713–724. Linear vibration analysis of laminated rectangular plates using the hierarchical finite element method, Part 2: forced vibration analysis.
27. A. Peano 1976 *Computers and Mathematics with Applications* **2**, 211–224. Hierarchies of conforming finite elements for plane elasticity and plane bending.
28. J. M. Whitney 1987 *Structural Analysis of Laminated Anisotropic Plates*. Lancaster: Technomic Publishing Co.
29. B. W. Char, K. O. Geddes, G. H. Gonnet, B. L. Leong, M. B. Monagan and S. M. Watt 1991 *Maple V Language Reference Manual*. New York: Springer-Verlag.
30. S. T. Chow, K. M. Liew and K. Y. Lam 1992 *Composite Structures* **20**, 213–226. Transverse vibration of symmetrically laminated composite plates.
31. *ESDU Data Item No*. 83086 1992 Natural frequencies of rectangular, specially orthotropic plates, ESDU International.

32. M. S. Qatu and A. W. Leissa 1991 *Composite Structures* **17**, 227–254. Natural frequencies for cantilevered doubly-curved laminated composite shallow shells.
33. N. C. Perkins and C. D. Mote Jr 1986 *Journal of Sound and Vibration* **106**, 451–463. Comments on curve veering in eigenvalue problems.
34. *ABAQUS User's Manual* (Version 5.5) 1995. Pawtucket, RI: Hibbit, Karlsson and Sorrensen.
35. W. Han and M. Petyt 1997 *Computers and Structures* **63**, 295–308. Geometrically nonlinear vibration analysis of thin rectangular plates using the hierarchical finite element method. Part 1: The fundamental mode of isotropic plates.
36. W. Han and M. Petyt 1997 *Computers and Structures* **63**, 309–318. Geometrically nonlinear vibration analysis of thin rectangular plates using the hierarchical finite element method. Part 2: first mode of laminated plates and higher modes of isotropic and laminated plates.